ARTICLES
https://doi.org/10.1038/s41560-018-0106-3
nature energy

# Quantitative experimental assessment of hot carrier-enhanced solar cells at room temperature

Dac-Trung Nguyen[1], Laurent Lombez[1,2*], François Gibelli[1,2], Soline Boyer-Richard[3], Alain Le Corre[3], Olivier Durand[3] and Jean-François Guillemoles[1,2]

**In common photovoltaic devices, the part of the incident energy above the absorption threshold quickly ends up as heat, which limits their maximum achievable efficiency to far below the thermodynamic limit for solar energy conversion. Conversely, the conversion of the excess kinetic energy of the photogenerated carriers into additional free energy would be sufficient to approach the thermodynamic limit. This is the principle of hot carrier devices. Unfortunately, such device operation in conditions relevant for utilization has never been evidenced. Here, we show that the quantitative thermodynamic study of the hot carrier population, with luminance measurements, allows us to discuss the hot carrier contribution to the solar cell performance. We demonstrate that the voltage and current can be enhanced in a semiconductor heterostructure due to the presence of the hot carrier population in a single InGaAsP quantum well at room temperature. These experimental results substantiate the potential of increasing photovoltaic performances in the hot carrier regime.**

Despite their current record power conversion efficiencies (PCEs)[1], solar cells are still far from their performance limits[2]. In a silicon solar cell, the mainstream technology, about 40% of the absorbed light energy is lost by thermalization. This is one of the main reasons explaining why the maximum achievable PCE of classical photovoltaic devices is governed by the Shockley–Queisser limit of about 31%[3]. Most of the efforts towards reaching the highest efficiencies possible are based on multijunction solar cells where each individual junction converts a fraction of the solar spectrum: in this approach, the average energy converted per junction is modest while the full device exhibits a substantial sensitivity to variations of the incident light spectrum. In theory, according to a previous study[4], a single-diode device can be as efficient as a multijunction device if dissipation of the carrier energy via heat can be avoided (that is, if the kinetic energy of the photogenerated hot carriers could be converted into additional free energy). Indeed, thermoelectric devices convert heat gradients into electrical energy and photovoltaic devices convert light flux into electrical energy. The high lattice thermal conductivity of usual semiconductors would generally prevent direct use of the thermoelectric effect[5]. To fight lattice conductivity, one option is to keep the lattice isothermal while only the photogenerated carriers can become hot[4,6]. Such decoupling of the lattice and carrier temperature has been observed in nanostructures, such as quantum well (QW) structures that have shown slower carrier cooling rates as compared to bulk materials[7–12].

Today, we find a plethora of promising studies on the development and characterization of hot carrier absorbers[13–20]. However, the optical methods used to obtain the carrier temperature can be inaccurate when dealing with nanostructures and high excitation fluxes[21–23]. Meanwhile, several studies have been performed towards completed devices, especially electrical investigation to validate energy selective contacts[24–27].

Here, we study a hot carrier device operating at room temperature under continuous wave illumination with direct measurement of the hot carrier population and assessment of its contribution to power conversion. For this purpose, we fabricated a QW-based p–i–n hot carrier solar cell prototype and investigated its optical and electrical properties. To investigate hot carrier effects, we have analysed photoluminescence (PL) and electroluminescence spectra from which one may extract thermodynamic quantities such as the temperature and the chemical potential of radiation (using the generalized Planck radiation law[28,29]); both are related to the carrier thermodynamic properties. We use a model of the absorption including excitons, free carriers and band filling, which allows us to fit the whole PL spectra over a large range of excitation powers[22,30]. Quantitative optical measurements indicate the presence of a hot carrier population within the QW. This gives an increase of the electrochemical potential in the barrier. Such an effect is analogous to a Seebeck conversion process[18]. The quantitative optical measurements are then compared to the electrical characteristics. The real impact of the hot carrier population within the structure is then discussed and quantified.

## QW hot carrier solar cell

The solar cell prototype is depicted in Fig. 1. The multilayer wafer contains a region with an intrinsic InGaAsP-based QW/barriers, which acts as the absorber generating hot carriers, while the barriers and claddings play the role of energy semi-selective contacts[14,31] (see Table 1). This absorber–contacts layer is sandwiched between two gradually n- and p-doped InP layers for carrier separation and collection.

Current–voltage characteristics are first recorded for cells with diameters ranging from 5 to 200 μm. The 11.0 ± 0.5-μm diameter cell shows the highest efficiency under continuous-wave laser excitation at 980 nm. The PCE is 11.6 ± 0.5% under focused laser illumination of 1,650 W cm$^{-2}$ (equivalent to 55,600 suns and close to the maximum achievable solar concentration, see Supplementary Notes 4–6 for more details). Although we measure efficiencies of potential hot carrier solar cells, the purpose of the design is to allow a proper optoelectrical measurement. The excellent electrical characteristics stem from an extremely low series resistance, which yields a short-circuit current that is proportional to the laser power within

[1]Institut Photovoltaique d'Ile de France (IPVF), Palaiseau, France. [2]CNRS-Institut Photovoltaique d'Ile de France (IPVF), UMR 9006, Palaiseau, France. [3]Univ Rennes, INSA Rennes, CNRS, Institut FOTON – UMR 6082, Rennes, France. *e-mail: laurent.lombez@cnrs.fr

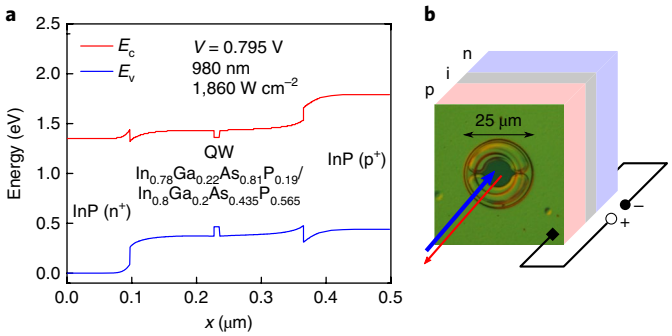


**Fig. 1 | Description of the hot carrier heterojunction device. a**, Energy band diagram of the heterostructure with a 980 nm excitation wavelength, 1,890 W cm$^{-2}$ and at open-circuit condition. $E_c$ ($E_v$) stands for the conduction (valence) energy band level. **b**, Top view of the micro-solar cell taken with an optical microscope (golden green) and schematic of the opto-electrical characterization (light red–grey–light blue). Charge carriers are generated by continuous-wave laser excitation at 980 nm (blue arrow) and the thermodynamic properties of the charge carriers are probed by the luminescence induced by radiative recombination (red arrow).

**Table 1 | Characteristics of the layers in the sample**

| Composition | Doping | Thickness | Role |
|---|---|---|---|
| InGaAs | p$^{++}$ | 170 nm | Electric contact |
| $In_{0.8}Ga_{0.2}As_{0.435}P_{0.565}$ | p$^+$ | 50 nm | |
| InP | p$^+$ | 50 nm | Cladding |
| $In_{0.8}Ga_{0.2}As_{0.435}P_{0.565}$ | i | 120 nm | Barrier |
| $In_{0.78}Ga_{0.222}As_{0.81}P_{0.19}$ | i | 7.4 nm | Quantum well |
| $In_{0.8}Ga_{0.2}As_{0.435}P_{0.565}$ | i | 130 nm | Barrier |
| InP | n$^+$ | 40 μm | Cladding |

The intrinsic (i) InGaAsP-based absorber consists of a 7.4 nm QW ($E_g$ = 0.78 eV) between 120 and 130 nm barriers ($E_g$ = 1.05 eV). The absorber is sandwiched between p- and n-doped InP contact layers.

the entire experimental range (see Fig. 2). The open-circuit voltage exceeds the lowest absorption threshold at laser fluences higher than ~6,000 W cm$^{-2}$, which would indicate a power conversion efficiency above that of an equivalent device in thermal equilibrium. To determine whether band filling contributes solely to this high conversion efficiency, further analyses are required as laid out in the following.

## Determination of carrier thermodynamic properties

Luminescence spectra, calibrated in absolute units, are recorded at room temperature and atmospheric pressure to determine the carrier thermodynamic properties. Indeed, the carrier temperature $T$ and the quasi-Fermi level splitting $\mu = E_{Fn} - E_{Fp}$ (where $E_{Fn}$ and $E_{Fp}$ are the electron and hole Fermi levels) are determined according to the generalized Planck law[22,29,32]:

$$\Phi(E) = \frac{2A(E) \times E^2}{h^3 c^2} \times \frac{1}{\exp\left(\frac{E-\mu}{k_B T}\right) - 1} \quad (1)$$

Here $\Phi$ is the luminescence emission, $E$ is the photon energy, $A(E)$ is the absorptivity, $h$ is the Planck constant, $c$ is the speed of light in a vacuum and $k_B$ is the Boltzmann constant.

Determination of the absorptivity $A(E)$ is crucial for minimizing the uncertainty in the evaluation of the thermodynamic properties $T$ and $\mu$ in equation (1) (see Methods and Supplementary Notes 1 and 2). Indeed, $A(E)$ might affect the whole spectral variation of the PL signal including the high energy range. To validate the model of the absorption in the sample structure, we compare the

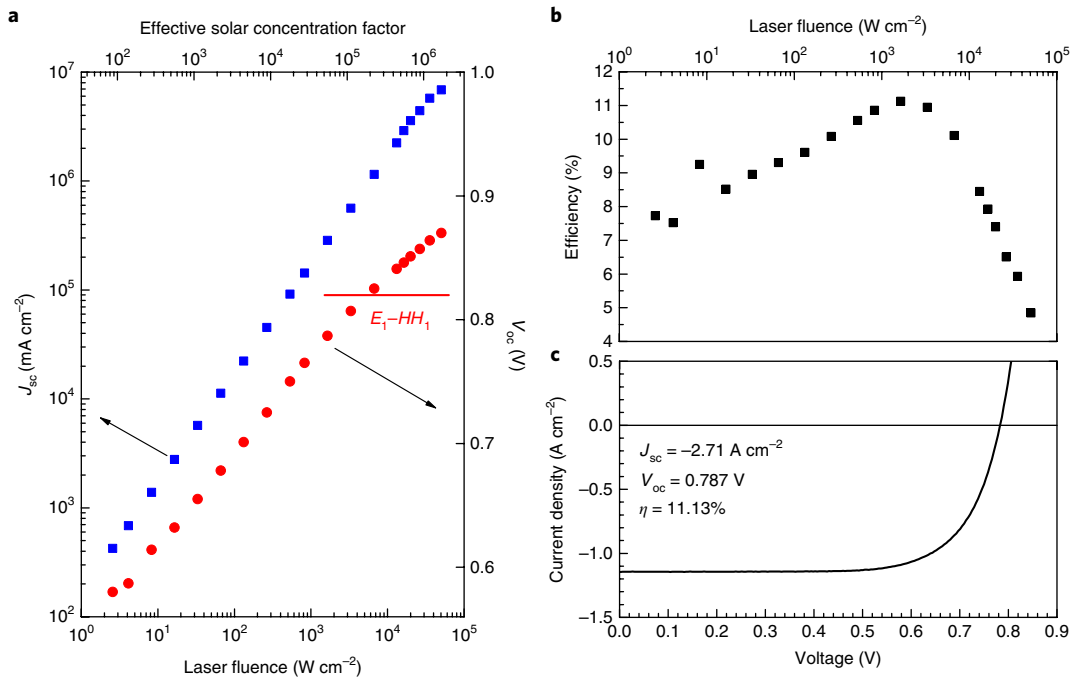


**Fig. 2 | Electrical characteristics of the heterojunction device. a**, Variation of short-circuit current density ($J_{sc}$, blue squares) and open-circuit voltage ($V_{oc}$, red circles) with laser power. The red horizontal line indicates the $E_1$–$HH_1$ transition energy. The indicative solar illumination concentration incident on the device is obtained by multiplying the laser fluence (in W cm$^{-2}$) by a factor of 33.7, as $J_{sc}$ = 4.5 mA cm$^{-2}$ was measured under AM1.5 solar spectrum excitation. Details on this conversion are given in Supplementary Note 6. **b**, Equivalent conversion efficiency as a function of the effective concentration with a 980 nm excitation wavelength. **c**, Current–voltage curve taken at the maximum efficiency ($\eta$).

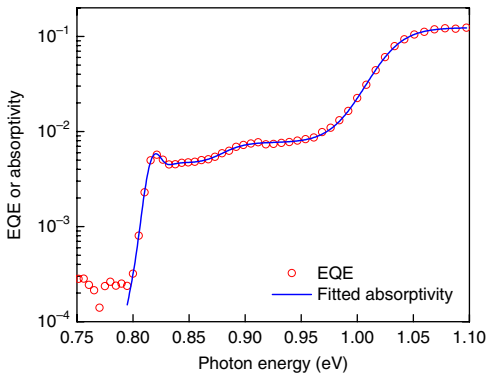


**Fig. 3 | EQE and absorption model.** Data are shown from 0.78 eV (1,550 nm) to 1.10 eV (1,127 nm) where absorption by the QW/barriers occurs. The EQE (red circles) is fitted using the expression of unsaturated absorptivity (blue line) $A_0(E) = (1-R)\{1-\exp[-(\alpha_{w0}d_w + \alpha_{b0}d_b)]\}$. The reflectivity $R$ is measured to be about 0.3 over the spectral range [0.75,1.10] eV. The absorption model includes QW interband excitonic and free-carrier absorption (in $\alpha_w$), as well as barrier interband absorption (in $\alpha_b$). See Supplementary Note 1 for more details on the QW/barrier absorption coefficients $\alpha_{w0}$ and $\alpha_{b0}$. The experimental data reflect both qualitatively and quantitatively the absorptivity obtained from PL measurements at low excitation power. The exciton peak is centred at 0.82 eV and the absorption plateaux are observed, corresponding to the fundamental and the first excited levels of the QW. The result is presented in detail in Supplementary Note 3.

absorptivity calculated from luminescence spectra with the external quantum efficiency (EQE; see Fig. 3). Indeed, if the collection of photo-generated carriers was lossless, the electric current density would correspond to the number of absorbed photons[28]. In the case of relatively shallow wells, as in our samples ($\Delta E_c \lesssim 0.2$ eV), the collection efficiency is generally found to be close to unity[33–35]. Hence, photocurrent can be used as an indirect measure of the absorption. We found a good agreement between the EQE and $A(E)$ obtained from our model.

Therefore, luminescence spectra at different laser excitation powers and different applied voltages have been recorded and analysed. In all cases, the full-spectrum fit is in good agreement with the experimental data, as can be seen in Figs. 4 and 5.

We optically probe the carrier thermodynamic properties in both the barrier and the QW spectral regions (see Supplementary Note 7 for detailed results). Figure 4c shows the carrier temperature as a function of the excitation power. We observe a temperature increase of more than 1,000 K above room temperature for the carrier in the QW (that is, 1,000 K above the carrier temperature in the barrier)—a range of temperature already reported in the literature[21,23]. We have previously demonstrated that this surplus amount of heat can be converted into a gain in voltage via a Richardson emission of hot carriers (also seen as a pseudo-Seebeck effect)[18]. This is confirmed when looking at the electrochemical potentials of the carriers in both spectral regions (see Fig. 4d): the difference between the two values increases with the carrier temperature in the quantum well. Notably, the value of the electrochemical potential $\mu_b$ in the barrier

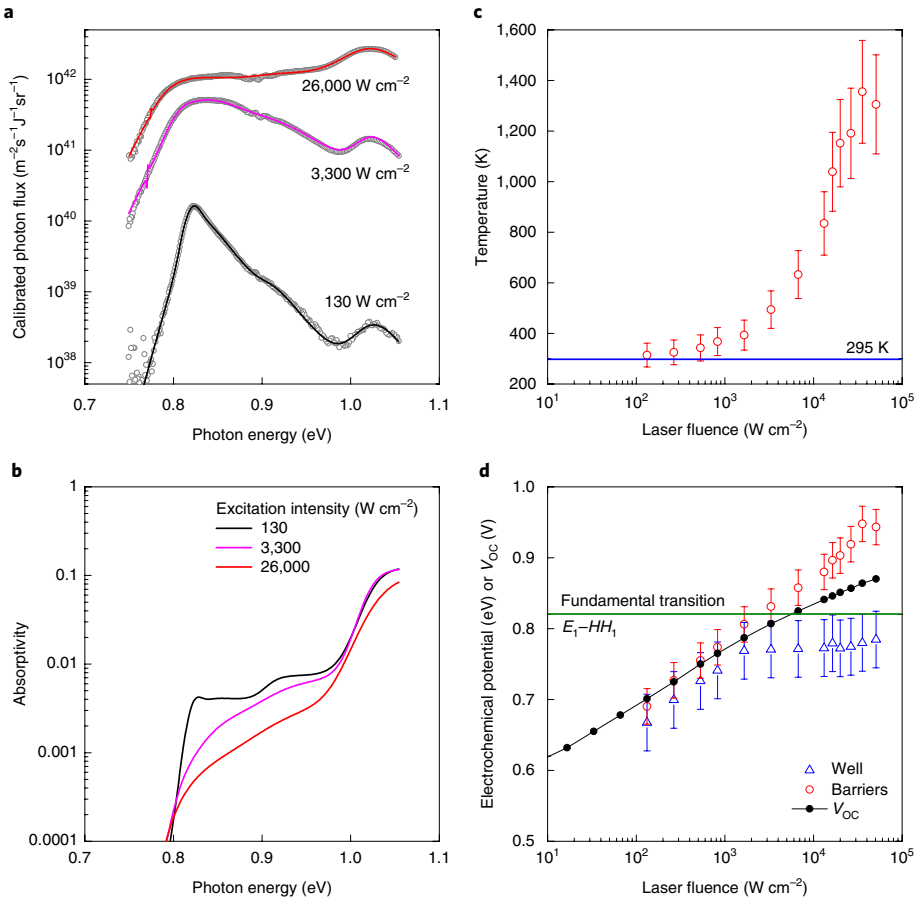


**Fig. 4 | Variation of carrier thermodynamic properties with laser intensity. a**, Three PL spectra (grey circles) and their fits at low (black line), medium (magenta line) and strong (red line) laser excitation, in the open-circuit regime. **b**, Corresponding absorptivity deduced from the fits. **c**,**d**, Variation of QW carrier temperature $T_w$ and electrochemical potentials in the QW $\mu_w$ (red circles) and barriers $\mu_b$ (blue triangles) with laser power. Evaluated uncertainties in the optical measurement are displayed by errors bars. See Methods for details on the evaluation of uncertainties.

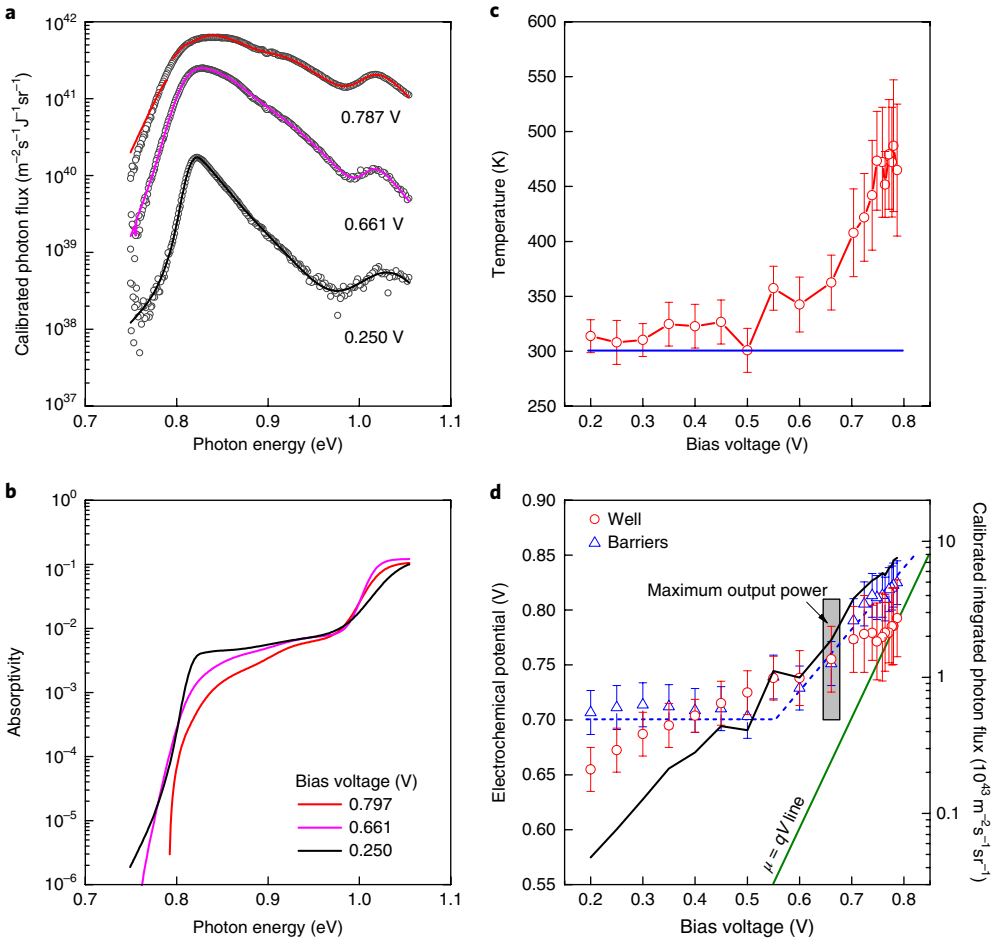


**Fig. 5 | Variation of carrier thermodynamic properties with bias voltage.** The laser intensity is 1,890 W cm$^{-2}$. **a**, Three PL spectra (grey circles) with respective fits (continuous lines) at three bias voltages: $V = 0.250$ V (black line), $V = 0.661$ V (magenta line) and $V = 0.787$ V (red line). **b**, Corresponding absorptivities deduced from the fits at the same bias voltages. **c**, Variation of carrier temperature in the QW (red circles) with bias voltage. The blue line represents ambient temperature around 297 K. **d**, Variation of electrochemical potential in the QW (red circles) and barriers (blue triangles), and of luminescence intensity (black continuous line) with bias voltage. The dashed blue line serves as a visual guide for the variation of the barriers' electrochemical potential and the green continuous line depicts the $\mu = qV$ dependence. The grey box highlights the maximum output power working point. The evaluation of uncertainties is detailed in the Methods.

region exceeds the lowest absorption threshold of the QW (0.82 eV), which is consistent with the electrical response we observe.

The determined absorptivities for three laser excitation powers are shown in Fig. 4b. One can infer that saturation of absorption in the QW region is only partial, which indicates that the QW would be still optically active for absorption. This observation supports the hypothesis that the increase in the electrochemical potential in the QW $\mu_b$ is linked to a hot carrier effect rather than a band-filling phenomenon. Therefore, the fact that $\mu_b$ is higher than the fundamental transition $E_1$–$HH_1$ would indeed indicate that the barriers are allowing for isentropic cooling of the carriers, which corroborates hot carrier solar cell functionality.

We then carried out luminescence experiments under an electric bias to quantify the contribution of this hot carrier effect in the obtained device characteristics. As in Fig. 4, we display in Fig. 5 fits of biased-PL spectra, absorptivity and evolution of the thermodynamic quantities with the applied voltage (see Supplementary Note 8 for detailed results). The incident laser excitation power is set to 1,890 W cm$^{-2}$. All of the measurements are carried out in a collection regime, at applied bias lower than the $V_{oc} = 0.795$ V. In such an optoelectrical experiment, one might expect values of $\mu_b$ close to the applied bias, as the carriers in this spectral region are supposed to be cold (that is, fast thermalization). The green line in Fig. 5d shows the condition where $V = \mu/q$ ($q$, elementary charge). The electrochemical potential $\mu_b$ in our case is found to be slightly higher than the applied voltage (see Fig. 5d blue triangles) and two different regimes can be distinguished. Below a bias voltage $V = 0.6$ V, we see a rather constant value of $\mu_b$ around 0.7 eV, which then increases for higher bias voltages. This can be explained by a weak carrier collection efficiency at high excitation intensities. The effect is confirmed by the observation of a PL signal at all biases, although all of the carriers would have been electrically collected (see Fig. 5d blue lines). The luminescence signal under bias is the sum of the electroluminescence and PL signal at short-circuit current[28], the latter being small but non-negligible in our case.

Fixing the laser intensity to a high value and starting at the open-circuit condition, we would expect $T$ and $\mu$ to decrease in the QW region with decreasing bias voltage (that is, we reduce the carrier density by extracting carriers as expected) as illustrated by the results presented in Fig. 5 as the bias voltage is varied from 0.8 V to 0.6 V. Thermodynamic values below 0.6 V are once again affected by a reduced carrier collection efficiency.

## Contribution of hot carriers to voltage and current gains

A key point in the last experiment is to probe the hot carrier effect at the maximum power point, which is found at 0.651 V (grey zone

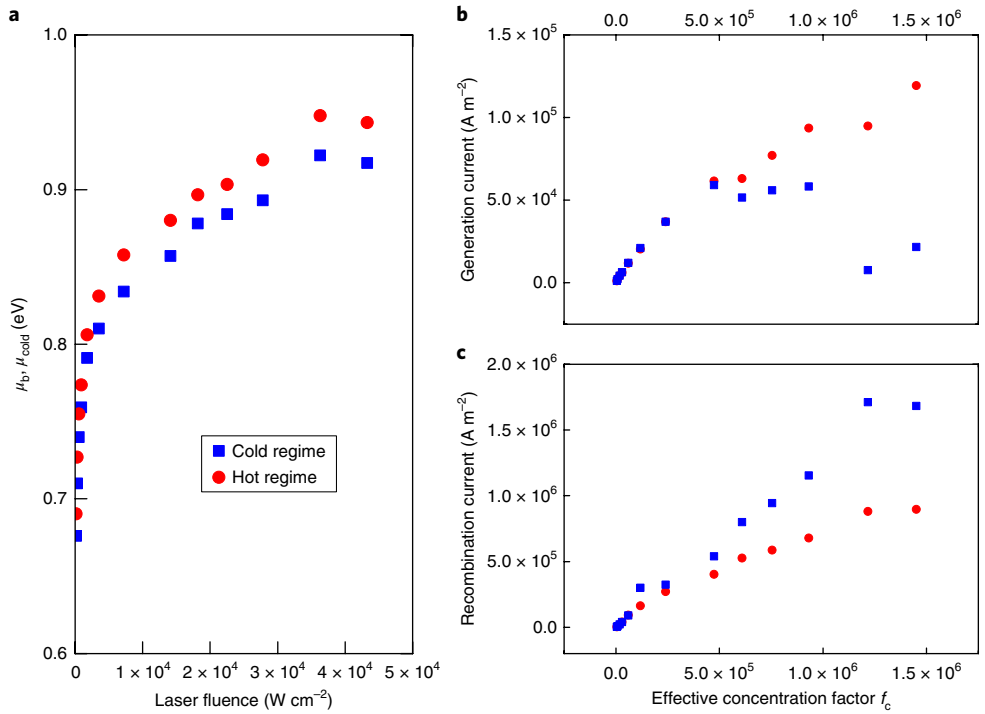


**Fig. 6 | Assessment of the hot carriers' contribution to power generation.** Evaluation of the hot carrier contribution on the electrical properties of the cell with the excitation intensity. **a**–**c**, Evolution of the electrochemical potential (**a**), generation current (**b**) and recombination current (**c**) in the hot carrier regime (red dots) and cold carrier regime (blue squares).

highlighted in Fig. 5d). With the laser excitation condition used here (1,890 W cm$^{-2}$ on a 11-µm-diameter cell), we obtain a PCE of 11.6%. Here, the electrochemical potential increases from $\mu_w$ to $\mu_b$ by 110 mV, and 50 mV for the maximum power point, showing an efficient conversion of the temperature difference into electrochemical potential difference[18]. Still, we need to estimate the hot carrier contribution to the total voltage and current.

In a first-step approach, we propose to compare the open-circuit voltage in a hot and cold carrier regime. We assess the contribution of the well to the power conversion as a function of the hot carriers' temperature, using the fact that the hot carriers are essentially in the well. Two situations are considered: the experimental scenario for which hot carriers are produced in the well, and where the electrochemical potential is known in the barriers; and a virtual situation in which the carriers in the well would be cold and in equilibrium with those in the barrier. This situation can be simulated using our fitting parameters (see Supplementary Note 9). Figure 6a shows the evolution of $\mu_b$ (that is, the maximum achievable voltage for the case of hot carriers) and the calculated one $\mu_{cold}$ for the case of cold carriers. We assumed here the same radiative efficiency in both cases and find the quasi Fermi level splitting in the barriers to be larger by about 25 to 30 meV with hot carriers as compared to the case of lattice thermalized carriers (see Fig. 6a). The same simulation in the experiment under bias (and lower laser excitation power) shows an increase of the quasi-Fermi level splitting by about 10 meV for $V > 0.65$ V (that is, where hot carriers are present). This is a strong indication of a voltage gain from the conversion of the hot carriers' thermal energy.

In the next step, we probe whether there is any possible gain in current. Although the experiments presented here give a clear picture of the physical phenomena at work, they do not exactly correspond to the operation of a solar cell. To understand the impact of hot carriers in a heterostructure on the conversion of solar energy, it is necessary to extrapolate the previous described case (that is, the laser excites only transitions in the barriers) to the case where the solar spectrum excites all optical transitions. In the former case, transitions from the well contribute only to the recombination current while in the latter case they also contribute to the photocurrent. The key point is whether the balance between the additional generation and recombination due to the presence of the well yields a positive contribution to solar energy conversion or not.

To assess the contribution of the well to current generation, we propose a metric to consider the marginal gain (additional generation) versus the marginal loss (additional recombination) induced by the well at a given operating point. Subsequently, we evaluate this metric in the presence as well as in the absence of hot carriers. The entire procedure is detailed in Supplementary Note 9. On the one hand, the marginal generation is computed for a solar spectrum at a concentration yielding the same photocurrent as measured at the considered working point. We use the measured absorptivity in the spectral range where only well transitions contribute (for example, $E < 1.1$ eV). As shown in Fig. 6b, the photogenerated generation current increases in the presence of hot carriers and is always higher than the generation current in the equilibrium case (that is, cold carriers). In that case, the current vanishes because of the net absorption reduction where stimulated emission could occur (that is, strong band-filling effect)[32].

On the other hand, the marginal recombination was computed from radiative recombination assuming a radiative yield (see Fig. 6c). The recombination current increases in both the hot and the cold regime, with the cold regime yielding higher values. Finally, to probe what would be the contribution of current due to the QW in the case of a solar spectrum illumination, we need to subtract the generation current from the recombination current. This gain is much more pronounced in the hot regime. Therefore, the presence of hot carriers is essential for the QW region to act as a current generator.

This finding is very promising since the present structure suffers from weak absorption in the barrier and, more importantly, in

the single well (which collects only ≲1% of the incident light, see Figs. 4b and 5b, a value comparable to monolayers of two-dimensional materials such as graphene). Here, light management in the cell would be beneficial for reducing the effective concentration for the same amount of generated current and thus increase the impact of the QW in solar energy conversion.

## Conclusion

We investigated a p–i–n single-QW device by means of complementary optical and electrical measurements. Our device exhibits its maximum efficiency at incident powers equivalent to 50,000 suns (that is, one order of magnitude higher than the current achievement in concentrator photovoltaics). Electrical measurements show $V_{oc}$ to be above the minimum absorption threshold, which could indicate a working condition for this device above the limit for classical device operation where thermal equilibrium is present. To clarify this observation, the variation of the carrier thermodynamic properties as a function of optical excitation power or electrical bias is determined by a rigorous fit of the complete luminescence spectra. The optical measurements confirm the electrical behaviour and allow us to quantify the impact of hot carriers on device functionality. A striking observation is that voltage and current enhancements are observed due to the presence of hot carriers. These findings exemplify that current state-of-the-art semiconductor heterostructures can already be used to boost solar energy conversion by hot carrier mechanisms. The present results will be instrumental to designing a new generation of devices for enhancing the hot carrier conversion contribution, both optically and electrically.

## Methods

**Sample preparation and hyperspectral imaging.** The investigated sample is based on a quaternary $In_xGa_{1-x}As_yP_{1-y}$ compound grown on lattice-matched InP substrate. The layer compositions and thicknesses are given in Fig. 1. The wafer structure has been optimized from the results of our previous work[5] that optically showed evidence of hot carrier effects in a QW/barriers absorber. The multilayer wafer contains an intrinsic InGaAsP-based QW/barriers region, playing the role of an absorber that generates hot charge carriers. The barriers play the role of semi-selective contacts where the carriers are mainly cold. This well/barriers region is sandwiched between two gradually n- and p-doped InP layers for carrier separation and collection. The QW has been designed to minimize the number of energy levels in the QW and to spectrally separate absorption in the quantum well and in the barriers, to simplify the spectral analysis. Band structures calculated from k.p formalism are shown in Supplementary Fig. 1, indicating that a single optical transition is dominant in the QW region.

In our experimental set-up, a hyperspectral imaging system from Photon Etc. records quantitative luminescence spectra (luminance), which we subsequently calibrate to obtain absolute values. This allows us to evaluate the emission thermodynamic properties, which are related to the carrier thermodynamic properties. The excitation laser wavelength is 980 nm. All measurements are carried out at room temperature. More details on the experimental set-up are provided in Supplementary Fig. 2.

**Modelling the absorption.** The absorptivity is calculated from absorption coefficients and layer thicknesses. For our well/barriers structure, we write:

$$A(E) = [1-R(E)] \times \{1-\exp[-(\alpha_w d_w + \alpha_b d_b)]\}$$

where $\alpha_w$ and $\alpha_b$ are the effective absorption coefficients of the well and barriers, and $d_w$ and $d_b$ are their thicknesses. We used an absorption model taking into account excitons and free carriers in the well, as well as free carriers in the barriers[22,36,37]. This effect of band filling[38] is expressed by introducing occupation functions into the absorption coefficient $\alpha_s = \alpha_0 \times [f_v^e(E_h) - f_c^e(E_e)]$. Detailed expressions of absorption are provided in Supplementary Notes 1 and 2.

**Evaluation of uncertainties in optical measurements.** The temperature $T$ and electrochemical potential $\mu$ are determined from fits of the luminescence spectra. Uncertainties, in the measurement of $T$ for example, are evaluated by manually assigning it to a fixed value $T$ around its fitted value $T_0$ and launching the fit again, until the fitted spectrum becomes unsatisfactory. Mathematically, that means ~10% or more of the points in the fitted luminescence spectrum present a relative error $|\Phi_{fit}(T) - \Phi_{exp}|/\Phi_{exp}$ of at least ~10% compared to experimental data.

**Data availability.** The data that support the plots within this paper and other findings of this study are available from the corresponding author upon reasonable request.

Received: 20 September 2017; Accepted: 26 January 2018;
Published online: 6 March 2018

## References

1. Green, M. A. et al. Solar cell efficiency tables (version 50). *Prog. Photovolt. Res. Appl.* **25**, 668–676 (2017).
2. Green, M. A. *Third Generation Photovoltaics* (Springer-Verlag, Berlin/Heidelberg, 2006).
3. Shockley, W. & Queisser, H. J. Detailed balance limit of efficiency of p-n junction solar cells. *J. Appl. Phys.* **32**, 510–519 (1961).
4. Ross, R. T. & Nozik, A. J. Efficiency of hot-carrier solar energy converters. *J. Appl. Phys.* **53**, 3813–3818 (1982).
5. Kettemann, S. & Guillemoles, J.-F. Thermoelectric field effects in low-dimensional structure solar cells. *Phys. E Low Dimens. Syst. Nanostruct.* **14**, 101–106 (2002).
6. Würfel, P. Solar energy conversion with hot electrons from impact ionisation. *Sol. Energy Mater. Sol. Cells* **46**, 43–52 (1997).
7. Rosenwaks, Y. et al. Hot-carrier cooling in GaAs: Quantum wells versus bulk. *Phys. Rev. B* **48**, 14675–14678 (1993).
8. Xu, Z. Y. & Tang, C. L. Picosecond relaxation of hot carriers in highly photoexcited bulk GaAs and GaAs-AlGaAs multiple quantum wells. *Appl. Phys. Lett.* **44**, 692–694 (1984).
9. Ryan, J. F. Time-resolved photoluminescence of two-dimensional hot carriers in GaAs-AlGaAs heterostructures. *Phys. Rev. Lett.* **53**, 1841–1844 (1984).
10. Shah, J. Energy-loss rates for hot electrons and holes in GaAs quantum wells. *Phys. Rev. Lett.* **54**, 2045–2048 (1985).
11. Leo, K. Reduced dimensionality of hot-carrier relaxation in GaAs quantum wells. *Phys. Rev. B* **37**, 7121–7124 (1988).
12. Lugli, P. Nonequilibrium longitudinal-optical phonon effects in GaAs-AlGaAs quantum wells. *Phys. Rev. Lett.* **59**, 716–719 (1987).
13. Conibeer, G. et al. Modelling of hot carrier solar cell absorbers. *Sol. Energy Mater. Sol. Cells* **94**, 1516–1521 (2010).
14. Le Bris, A. & Guillemoles, J.-F. Hot carrier solar cells: Achievable efficiency accounting for heat losses in the absorber and through contacts. *Appl. Phys. Lett.* **97**, 113506 (2010).
15. Le Bris, A. et al. Thermalisation rate study of GaSb-based heterostructures by continuous wave photoluminescence and their potential as hot carrier solar cell absorbers. *Energy Environ. Sci.* **5**, 6225–6232 (2012).
16. Le Bris, A. et al. Hot carrier solar cells: controlling thermalization in ultrathin devices. *IEEE J. Photovolt.* **2**, 506–511 (2012).
17. Hirst, L. C., Walters, R. J., Führer, M. F. & Ekins-Daukes, N. J. Experimental demonstration of hot-carrier photo-current in an InGaAs quantum well solar cell. *Appl. Phys. Lett.* **104**, 231115 (2014).
18. Rodière, J., Lombez, L., Le Corre, A., Durand, O. & Guillemoles, J.-F. Experimental evidence of hot carriers solar cell operation in multi-quantum wells heterostructures. *Appl. Phys. Lett.* **106**, 183901 (2015).
19. Esmaielpour, H. et al. Suppression of phonon-mediated hot carrier relaxation in type-II InAs/$AlAs_xSb_{1-x}$ quantum wells: a practical route to hot carrier solar cells. *Prog. Photovolt. Res. Appl.* **24**, 591–599 (2016).
20. Zhang, Y. et al. Extended hot carrier lifetimes observed in bulk $In_{0.265\pm0.02}Ga_{0.735}N$ under high-density photoexcitation. *Appl. Phys. Lett.* **108**, 131904 (2016).
21. Tedeschi, D. et al. Long-lived hot carriers in III–V nanowires. *Nano Lett.* **16**, 3085–3093 (2016).
22. Gibelli, F., Lombez, L. & Guillemoles, J.-F. Accurate radiation temperature and chemical potential from quantitative photoluminescence analysis of hot carrier populations. *J. Phys. Condens. Matter* **29**, 06LT02 (2017).
23. Esmaielpour, H. et al. Effect of occupation of the excited states and phonon broadening on the determination of the hot carrier temperature from continuous wave photoluminescence in InGaAsP quantum well absorbers. *Prog. Photovolt. Res. Appl.* **25**, 782–790 (2017).
24. Dimmock, J. A. R., Day, S., Kauer, M., Smith, K. & Heffernan, J. Demonstration of a hot-carrier photovoltaic cell. *Prog. Photovolt. Res. Appl.* **22**, 151–160 (2014).
25. Dimmock, J. A. R. et al. Optoelectronic characterization of carrier extraction in a hot carrier photovoltaic cell structure. *J. Opt.* **18**, 074003 (2016).
26. Julian, A., Jehl, Z., Miyashita, N., Okada, Y. & Guillemoles, J. F. Insights on energy selective contacts for thermal energy harvesting using double resonant tunneling contacts and numerical modeling. *Superlattices Microstruct.* **100**, 749–756 (2016).
27. Hanna, M. C., Zhenghao, L. & Nozik, A. J. Hot carrier solar cells. *AIP Conf. Proc.* **404**, 309 (1997).
28. Rau, U. Superposition and reciprocity in the electroluminescence and photoluminescence of solar cells. *IEEE J. Photovolt.* **2**, 169–172 (2012).
29. Lasher, G. & Stern, F. Spontaneous and stimulated recombination radiation in semiconductors. *Phys. Rev.* **133**, A553–A563 (1964).
30. Gibelli, F., Lombez, L. & Guillemoles, J.-F. Two carrier temperatures non-equilibrium generalized Planck law for semiconductors. *Phys. B Condens. Matter* **498**, 7–14 (2016).

31. Feng, Y. et al. Non-ideal energy selective contacts and their effect on the performance of a hot carrier solar cell with an indium nitride absorber. *Appl. Phys. Lett.* **100**, 053502 (2012).
32. Würfel, P. The chemical potential of radiation. *J. Phys. C Solid State Phys.* **15**, 3967–3985 (1982).
33. Tsui, E., Nelson, J., Barnham, K., Button, C. & Roberts, J. S. Determination of the quasi-Fermi-level separation in single-quantum-well p-i-n diodes. *J. Appl. Phys.* **80**, 4599–4603 (1996).
34. Kluftinger, B., Barnham, K., Nelson, J., Foxon, T. & Cheng, T. Temperature-dependent study of the radiative losses in double-quantum well solar cells. *Sol. Energy Mater. Sol. Cells* **66**, 501–509 (2001).
35. Nelson, J., Paxman, M., Barnham, K. W. J., Roberts, J. S. & Button, C. Steady-state carrier escape from single quantum wells. *IEEE J. Quantum Electron.* **29**, 1460–1468 (1993).
36. Chemla, D., Miller, D., Smith, P., Gossard, A. & Wiegmann, W. Room temperature excitonic nonlinear absorption and refraction in GaAs/AlGaAs multiple quantum well structures. *IEEE J. Quantum Electron.***20**, 265–275 (1984).
37. Colocci, M., Gurioli, M. & Vinattieri, A. Thermal ionization of excitons in GaAs/AlGaAs quantum well structures. *J. Appl. Phys.* **68**, 2809–2812 (1990).
38. Zitter, R. N. Saturated optical absorption through band filling in semiconductors. *Appl. Phys. Lett.* **14**, 73–74 (1969).

## Acknowledgements

This work was carried out in the framework of a project of the IPVF (Institut Photovoltaïque d'Île-de-France). This project has been supported by the French Government in the framework of the programme of investment for the future (Programme d'Investissement d'Avenir) ANR-IEED-002-0. The authors acknowledge J. Even for the energy band structure simulation, T. Batté and N. Chevalier for technical assistance on sample and device fabrication, and P. Schultz and J. Connolly for carefully reading the manuscript.

## Author contributions

J.-F.G. and L.L. planned the study; D.-T.N. acquired the data; D.-T.N., L.L. and F.G. contributed to data treatment; S.B.-R., A.L.-C. and O.D. designed and fabricated the samples; D.-T.N., L.L. and J.-F.G. contributed to data analysis and modelling and wrote the paper.

## Competing interests

The authors declare no competing interests.

## Additional information

**Supplementary information** is available for this paper at https://doi.org/10.1038/s41560-018-0106-3.

**Reprints and permissions information** is available at www.nature.com/reprints.

**Correspondence and requests for materials** should be addressed to L.L.

**Publisher's note:** Springer Nature remains neutral with regard to jurisdictional claims in published maps and institutional affiliations.